



Modeling and Simulation of a Solid Propellant Gas Generator for **Hypersonic Airbreathing Propulsion**

Daniil Kalaev¹, Antonella Ingenito²

Abstract

Gas generators play a central role in solid-propellant air-breathing propulsion systems, particularly in hypersonic vehicles where compactness, reliability, and thermal efficiency are crucial. Their function is to supply a controlled flow of hot gases that sustain combustion in the main chamber, directly influencing overall performance and stability. This study presents a validated methodology for designing gas generators for solid-propellant air-breathing hypersonic systems. A guasi-one-dimensional model is coupled with high-fidelity 3D CFD simulations to enable both rapid performance prediction and detailed flow analysis. A dynamic grain regression model, implemented via a User Defined Function based on Vielle's law, allows the simulation of evolving geometry in response to chamber pressure. Results show strong agreement between 1D and 3D models in predicting pressure, mass generation, and temperature evolution. A newly developed fuel-rich propellant demonstrated improved thermochemical performance and stable gas output, supporting integration with a ramjet combustor. This framework provides a foundation for future coupling with the main combustor and grain geometry optimization across various flight conditions.

Keywords: gas generator design, solid-propellant air-breathing propulsion, hypersonic vehicles, CFD simulation, fuel grain regression.

Nomenclature

Abbreviations

CC – Combustion Chamber

CFD - Computational Fluid Dynamics

GG - Gas Generator

SRM - Solid Rocket Motor

Symbols

 A_b – Burning area [m²]

 C_d - Discharge coefficient [-] Δt - Time step [s]

 Δx – Grain displacement [m]

 L_0 – Initial grain length [m]

 \dot{m}_g – Gas mass flow rate [kg/s]

 m_a - Grain mass [kg]

P - Pressure [Pa]

R - Grain radius [m]

 R_g — Specific gas constant [J/(kg·K)] T — Temperature [K]

 t_b - Available burning time [s]

V – Volume [m^3]

 V_c - Free chamber volume [m³]

 x_b - Regression depth [m]

 \dot{x}_b - Regression velocity [m/s] Y - Volumetric source term [kg/(m³·s)]

 γ – Specific heat ratio [-]

 ρ – Density [kg/m³]

1. Introduction

Gas generators play a crucial role in solid-propellant-based air-breathing propulsion, particularly in ducted rockets and solid-fuel-ramjets (SFRJs), where hot gases mix with an oxidizer and ignite in a secondary combustion chamber. Propulsion systems utilizing solid fuel gas generators offer several advantages over purely solid and liquid propulsion, including higher specific impulse, operational simplicity, system compactness, and self-containment. Recent research on gas generators has primarily focused on fuel formulation and experimental performance characterization, with relatively little attention paid

¹Sapienza University of Rome, daniil.kalaev@uniroma1.it

²Sapienza University of Rome, antonella.ingenito@uniroma1.it

to the systematic design of gas generators and their internal flow dynamics. Numerous studies have explored the development of new boron-based high-enthalpy fuel-rich solid propellants. The authors in [1] and [2] investigated boron-loaded HTPB formulations achieving successful ignition and combustion inside a hybrid gas generator [3], reporting increased performance over pure HTPB. Komornik and Gany introduced a hybrid gas generator concept utilizing a paraffin/oxygen system to provide improved throttle ability and dynamic control [4]. Similarly, the author of [5] explores different pressure control strategies to vary the grain regression rate of the solid-fuel gas generator, offering better throttleability and dynamic control of the propulsion system. A static combustion study of a fuel-rich gas generator was conducted by the authors of [6], using a boron-based grain formulation and varying exhaust parts shape to achieve a fuel-rich gas exhaust with the following secondary combustion in a blast tube, showing complete combustion of the fuel-rich gases. Nakayama et al. (2009) investigated the second-stage ram combustor of a solid fuel ducted rocket system, using CFD and static tests to show that air-fuel ratio distribution in the dome region critically affects self-ignition and stable ram combustion [7]. However, numerical-based studies of gas-generator chambers remain sparse, as well as their design methodology. Most studies in this area are limited to ram combustors and chemical grain compositions, overlooking the complex transient, multiphase, reactive flow phenomena occurring within the gas generator itself. To address these gaps, the current study proposes a design approach for gas generators that combines a time-resolved analytical model with high-fidelity CFD simulations to capture both global thermodynamic evolution and localized flow behavior. The dual modeling strategy provides a foundation for robust gas generator design, with the potential to support future developments in combined-cycle propulsion and reusable hypersonic technologies. The analysis is conducted through a two-tiered modeling approach. Initially, a quasi-one-dimensional (1D) numerical model is formulated by solving the governing conservation equations within the gas generator. This model captures the time-resolved pressurization process and the generation rate of combustion products, providing a first-order estimation of thermodynamic parameters critical for preliminary design and system integration. Subsequently, a three-dimensional (3D) Computational Fluid Dynamics (CFD) model is developed using the CONVERGE [8] software suite to perform a detailed simulation of the gas generator's internal flow and regression dynamics. A custom User Defined Function (UDF), based on Vielle's regression law, is implemented to dynamically update the solid fuel boundary as a function of local chamber pressure. This approach enables an accurate representation of fuel grain regression and time-dependent geometry evolution within the simulation framework.

2. Design and sizing of the gas generator

The gas generator is designed to supply the ramjet combustor with a continuous stream of hot, fuel-rich gases. Unlike conventional solid rocket motors, the generator operates under strongly fuel-rich conditions so that the exhaust is not fully oxidized but rather consists of a mixture of partially decomposed hydrocarbons, carbon monoxide, hydrogen, and other combustible fragments. These products act as a gaseous fuel supply for the ramjet, where they mix and react with the incoming air to sustain efficient combustion at supersonic flight conditions.

From a geometrical standpoint, the gas generator adopts a cigarette grain (end-burning configuration). In this layout the propellant surface is simply the cross-sectional area of the grain and remains constant during the entire operation, while the burning front regresses axially. As a consequence, the gas generator delivers an almost constant mass flow of hot fuel-rich products, which is an essential requirement for stable ramjet operation.

The main characteristics of such a gas generator can be summarized as:

- Production of a steady and controlled flow of hot gases,
- Exhaust mixture intentionally fuel-rich, providing reactive species to the ramjet combustor,
- Simple grain geometry with predictable regression and burn duration,
- Compact design, suitable for integration upstream of the ramjet mixing section.

The design and sizing of the gas generator are driven by the ramjet's fuel demand. In practice, the

generator must supply a given mass flow rate of fuel-rich gases at the appropriate temperature and pressure to ensure mixing and ignition with the incoming air.

For a cigarette grain, the burning surface is:

$$A_b = \pi R^2,$$

where R is the grain radius. Since A_b is constant, the mass generation rate depends only on the chamber pressure through the burn rate law:

$$\dot{m}_a = \rho_p A_b a P^n$$
.

In the same way, the chamber pressure of the gas generator directly depends on the nozzle throat area.

Reducing the throat area increases the chamber pressure, which in turn raises the propellant regression rate and the generated mass flow. Conversely, enlarging the throat area decreases the chamber pressure and reduces the mass flow rate.

Since the hot gases produced by the generator act as the fuel supply for the ramjet combustor, a variation of A_t results in a direct control of the fuel mass flow delivered to the ramjet. The final outcome is a modulation of the overall thrust of the propulsion system, achieved simply by adjusting the throat geometry of the gas generator.

The available burning time is determined by the initial grain length L_0 :

$$t_b = \frac{L_0}{\dot{x}_b},$$

with $\dot{x}_b = aP^n$.

3. Transient Monodimensional Model of a Gas Generator with Cigarette Grain

This section presents a transient lumped-parameter model for the internal ballistics of a solid-propellant gas generator with a cigarette grain configuration (end-burning). In this configuration, the burning surface is constant and equal to the cross-sectional area of the port, while the combustion front regresses axially with time. The model aims to predict the time evolution of the chamber pressure and the regression depth, based on the balance between mass generation and mass ejection through the nozzle.

The model is referred to as monodimensional (or 0-D lumped parameter) because all thermodynamic quantities inside the combustion chamber (pressure P, temperature T, density ρ_g) are assumed uniform in space and only dependent on time t. The geometry of the grain is described by a single variable, the regression depth $x_b(t)$, which represents the distance traveled by the burning front. Hence, the system is reduced to two coupled state variables: P(t) and $x_b(t)$.

The local regression velocity of the propellant follows Vieille's law:

$$\dot{x}_b(t) = a P^n(t), \tag{1}$$

where:

- $x_b(t)$ = regression depth [m],
- $\dot{x}_b(t)$ = regression velocity [m/s],
- a = empirical burn rate coefficient,
- n = pressure exponent,
- P(t) = chamber pressure [Pa].

The burning surface is constant and equal to the port cross-sectional area:

$$A_b = \pi R^2, \tag{2}$$

where R is the grain radius.

The free chamber volume evolves with the regression depth as:

$$V_c(t) = A_b x_b(t). (3)$$

Its time derivative is:

$$\frac{dV_c}{dt} = A_b \, \dot{x}_b(t). \tag{4}$$

The propellant mass consumption rate is:

$$\dot{m}_q(t) = \rho_p A_b \dot{x}_b(t), \tag{5}$$

where ρ_p is the solid propellant density.

Assuming choked flow at the throat, the mass flow rate expelled through the nozzle is:

$$\dot{m}_{noz}(P) = C_d A_t P \sqrt{\frac{\gamma}{R_g T_c}} \left(\frac{2}{\gamma + 1}\right)^{\frac{\gamma + 1}{2(\gamma - 1)}}, \tag{6}$$

where:

- C_d = discharge coefficient,
- A_t = nozzle throat area,
- γ = specific heat ratio,
- T_c = chamber temperature (assumed constant),
- $R_g = R_u/M$ = specific gas constant of the exhaust gases.

The chamber pressure evolution is obtained from the global mass balance inside the control volume. The total mass of gas inside the chamber is:

$$m_c(t) = \frac{P(t) V_c(t)}{R_q T_c}.$$
 (7)

The mass balance reads:

$$\frac{dm_c}{dt} = \dot{m}_g(t) - \dot{m}_{noz}(P). \tag{8}$$

Substituting the expression of $m_c(t)$:

$$\frac{d}{dt}\left(\frac{PV_c}{R_gT_c}\right) = \dot{m}_g - \dot{m}_{noz}(P). \tag{9}$$

Since R_qT_c is constant, this becomes:

$$\frac{dP}{dt}\frac{V_c}{R_qT_c} + \frac{P}{R_qT_c}\frac{dV_c}{dt} = \dot{m}_g - \dot{m}_{noz}(P). \tag{10}$$

Multiplying through by $\frac{R_gT_c}{V_c}$:

$$\frac{dP}{dt} + \frac{P}{V_c} \frac{dV_c}{dt} = \frac{R_g T_c}{V_c} (\dot{m}_g - \dot{m}_{noz}(P)). \tag{11}$$

Thus, the pressure ODE is:

$$\frac{dP}{dt} = \frac{R_g T_c}{V_c(t)} \left(\dot{m}_g - \dot{m}_{noz}(P) \right) - \frac{P}{V_c(t)} \frac{dV_c}{dt}. \tag{12}$$

Finally, substituting (3), (4), (5) and (1):

$$\frac{dP}{dt} = \frac{R_g T_c}{A_b x_b} \left(\rho_p A_b a P^n - \dot{m}_{noz}(P) \right) - \frac{P}{x_b} a P^n. \tag{13}$$

The complete system of ODEs describing the transient gas generator operation is:

$$\frac{dx_b}{dt} = aP^n, (14)$$

$$\frac{dP}{dt} = \frac{R_g T_c}{A_b x_b} \left(\rho_p A_b a P^n - \dot{m}_{noz}(P) \right) - \frac{P}{x_b} a P^n. \tag{15}$$

At steady state, the chamber pressure P_{eq} is obtained by imposing the condition:

$$\dot{m}_g = \dot{m}_{noz}(P_{eq}). \tag{16}$$

Substituting the expressions:

$$\rho_p A_b a P_{eq}^n = C_d A_t P_{eq} \sqrt{\frac{\gamma}{R_g T_c}} \left(\frac{2}{\gamma + 1}\right)^{\frac{\gamma + 1}{2(\gamma - 1)}}.$$
(17)

Rearranging:

$$P_{eq}^{n-1} = \frac{C_d A_t}{\rho_p A_b a} \sqrt{\frac{\gamma}{R_q T_c}} \left(\frac{2}{\gamma + 1}\right)^{\frac{\gamma + 1}{2(\gamma - 1)}}.$$
 (18)

Thus the theoretical equilibrium pressure is:

$$P_{eq} = \left[\frac{C_d A_t}{\rho_p A_b a} \sqrt{\frac{\gamma}{R_g T_c}} \left(\frac{2}{\gamma + 1} \right)^{\frac{\gamma + 1}{2(\gamma - 1)}} \right]^{\frac{1}{n - 1}}.$$
 (19)

3.1. Choice of grain composition

The gas generator solid fuel grain composition used in this study is based on the fuel-rich composite propellant presented by Velari et al. [9], which was designed to be used in an artillery shell ramjet propulsion system. This formulation aims to produce a highly fuel-rich exhaust, comprising both reactive gas-phase species and condensed-phase aluminum compounds, suitable for downstream combustion in a secondary ramjet combustor. Such a concept is directly analogous to the solid gas generator-ramjet propulsion system discussed in this study.

The selected mixture is reported in the Table 1, and it has a density $\rho_p = 1531$ kg/m³.

Table 1. Composite propellant formulations and corresponding test pressures

Propellant	Binder %	AP Oxidizer %	Metal %	Pressure (bar)
Aluminum-based	35%	35%	30%	10, 30, 80, 100

The propellant binder consists of 77% hydroxyl-terminated polybutadiene (HTPB), 15% Di-octyl adipate (DOA), and 8% isophorone disocyanate (IPDI).

As the gas generator is designed to operate across a wide range of chamber pressures, enabling a variable grain regression rate, the exhaust gas compositions were analyzed using NASA's Chemical Equilibrium with Applications (CEA) code to estimate the thermodynamic properties and species distributions under equilibrium conditions.

The mole fractions of the exhaust gas species are reported in Table 2, and Figure 1 for easier interpretation. The species whose mole fraction falls below 1% is omitted. The high content of H_2 and CO

S. no	Product	10 bar	30 bar	80 bar	(100 bar)
1	AICI	0.05091	0.04961	0.04744	0.04671
2	СО	0.11937	0.1047	0.09434	0.09171
3	H_2	0.41889	0.41787	0.41535	0.41448
4	ALN(L)	0.05612	0.05499	0.05303	0.05245
5	$Al_2O_3(a)$	0.03273	0.03939	0.04395	0.04509
6	C(gr)	0.30252	0.31609	0.32429	0.32627

Table 2. Mole fractions of combustion products at different pressures

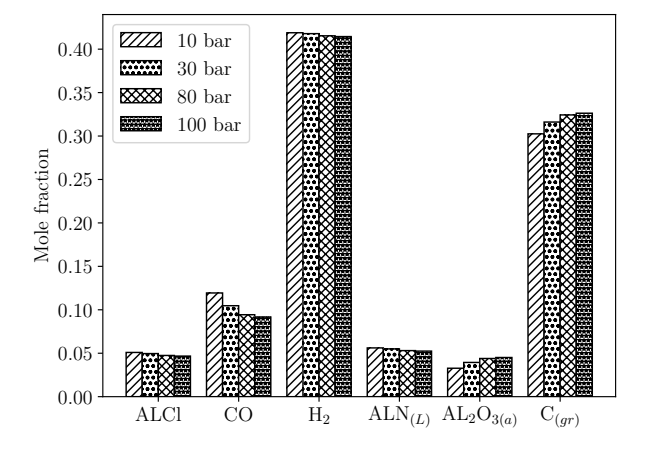


Fig 1. Exhaust composition of the solid grain for different chamber pressures

is ideal for secondary combustion in the ramjet. The exhaust gases also feature a significant portion of condensed-phase aluminum compounds like aluminum nitride $ALN_{(L)}$, and alumina $AL_2O_{3(a)}$, acting as latent energy carriers. In the oxidizer-rich ramjet combustor, those aluminum compounds burn, contributing to more thermal energy release and momentum via gas phase expansion. Fully burned aluminum will boost the specific impulse and total enthalpy. However, condensed-phase particles may agglomerate or cause erosion, thus both the gas generator and ramjet nozzles have to be designed with multiphase flow management in mind.

A high content of condensed carbon C_{gr} is also observed in the combustion products. This behavior is typical of fuel-rich propellant mixtures, where carbon available for oxidation is in great excess. Graphite formation is problematic in combustion systems, causing agglomeration, component erosion, and inefficient burning in ramjets due to slow oxidation and short residence times [10]. Increasing the chamber pressure generally promotes a shift toward greater formation of condensed-phase species in the exhaust.

The burn rate law for this propellant composition is given in Equation 20, which follows Vieille's law - an empirical relationship that describes how the burning rate of a solid propellant depends on the local pressure:

$$\dot{x}_b[mm/s] = 0.7 \cdot P[bar]^{0.45}$$
 (20)

In this expression, A=0.7 and n=0.45 are empirical constants determined for the aluminum–HTPB–AP formulation used in this study. These coefficients are valid over a chamber pressure range of 20 to 70 bar, and reflect the expected dependence of the regression rate on pressure. Exhaust gas conditions for different pressure values are reported in Table 3.

Property	10 bar	30 bar	80 bar	100 bar
Chamber Temp T_{CC} [K]	2327.0	2446.3	2558.2	2584.3
Specific heats ratio γ	0.868	1.094	1.091	1.090
MW [g/mol]	17.5	17.67	17.85	17.92

Table 3. Chamber conditions at 10–100 bar from CEA

3.2. Gas Generator Geometry and Computational Domain Description

As can be seen from Figure 2, the designed gas generator consists of two main regions: the solid fuel grain (in white) and the empty chamber located ahead of it. The latter includes a converging prenozzle cavity to help guide the flow, as well as a constant cross-section throat duct, which is connected downstream to the ramjet combustion chamber.

As the solid fuel burns, more volume is made available inside the chamber. The grain configuration is an end-burning cigarette grain with a constant burning surface area. As the propellant burns, the hot

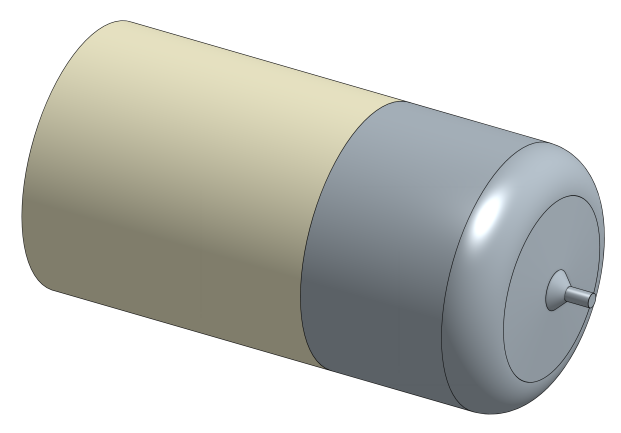


Fig 2. Model of the designed gas generator

gases are expelled through the nozzle, reaching choked flow conditions at the throat. As a result, the chamber becomes pressurized, providing a steady supply of exhaust gases while maintaining a fixed grain regression rate.

The computational domain used for the CFD analysis is shown in Figure 3. It corresponds to a 30° axisymmetric sector of the gas generator, with a 300 mm-long outlet section extending downstream of the chamber exit. The solid grain geometry is not explicitly included in the mesh; instead, it is embedded through a User-Defined Function (UDF) that governs the regression of the propellant surface. This configuration was selected to reduce the computational cost of the simulation by exploiting the axial symmetry of the flow field. A more detailed drawing of the computational domain used is presented in Figure 4, where the grain-fluid interface wall is modeled as a moving boundary whose motion is governed by the UDF.

The base mesh size in all directions was set to dx, dy, dz = 0.005 m. Fixed embeddings were applied at the grain–fluid interface with a scale factor of 2 and two embedded layers, and in the convergent and

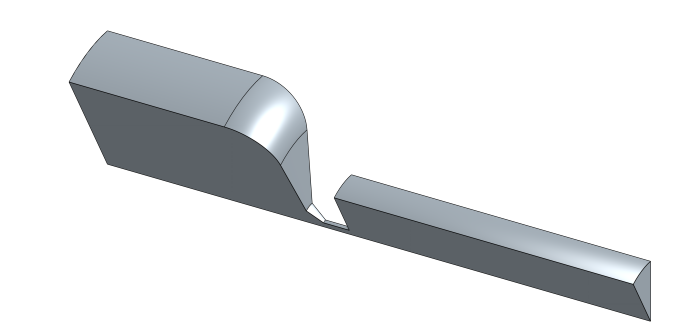


Fig 3. The computational domain of the gas generator study

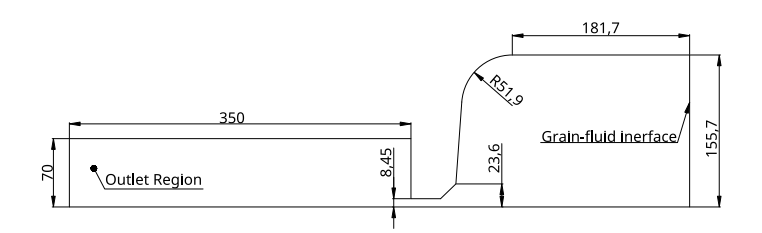


Fig 4. Computational domain dimensions in mm

constant sections of the nozzle with a scale factor of 2. Given the low flow velocities in the combustion chamber region, a coarser mesh resolution was maintained in this area.

3.3. Governing Models and Boundary Conditions

The gas generator simulation was performed using the CONVERGE CFD software suite, solving the compressible, and unsteady Navier–Stokes equations with axisymmetric assumptions. The flow was modeled as turbulent using the standard $k-\epsilon$ RANS model. The effects of the wall were treated using wall functions, ensuring the value of y+ in the range 30 < y+ < 200. The gas phase was modeled as an ideal gas, with temperature-dependent properties extracted from NASA CEA. In this study, no finite-rate chemical kinetics or chemical equilibrium models were used. Instead, the exhaust gases were injected as a time-dependent volumetric source at the grain-fluid interface. The composition of this composite species is reported in Table 2, at chamber temperature $T_{CC}=2446$ K, which corresponds to a chamber pressure of $P_{CC}=30$ bar, from the CEA analysis. The use of a single composite species, made up of mass fractions of the exhaust gases reported in Table 2, is beneficial at this stage as it allows the computational complexity of the problem to be reduced by solving a transport equation of only one species.

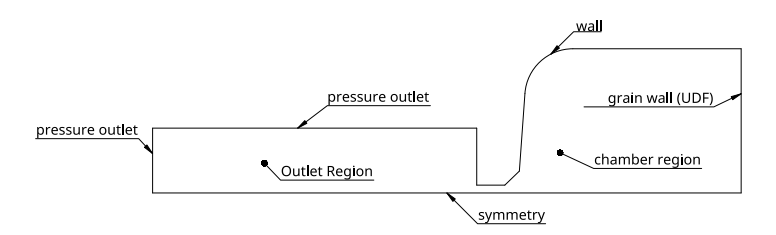


Fig 5. Boundary types and regions of the domain

The boundaries are labeled as reported in Figure 5. The boundary "symmetry" refers to the wall surfaces that form the sector of the computational domain and are modeled as boundary conditions of symmetry. The two " $pressure\ outlet$ " boundaries were set to a value slightly lower than the pressure expected at

the gas generator nozzle throat, namely $P_{out}=1.5~{\rm MPa}$. The same pressure value was also applied as the initial condition in the outlet region. This approach was adopted to prevent the occurrence of strong plume expansion downstream of the gas generator and the associated formation of shockwave patterns, which would otherwise require stricter mesh refinement and smaller time steps to maintain numerical stability. As the focus of this work is on accurately predicting the internal conditions of the gas generator chamber through the implementation of the dynamic UDF, and not on resolving the external jet flow, such simplification was considered appropriate.

The "wall" boundary is treated with the law of the wall boundary condition for velocity, and adiabatic for temperature. The " $chamber\ region$ " initial condition was set to the expected chamber pressure of $P_{CC}=3.0$ MPa. This initial condition was chosen to smooth out the initial transient peak in the gas generator chamber and to have the chamber conditions close to their final performance values. While the initial transient peak is of interest for modelling its behaviour accurately, it was not the focus of this study, as the presented gas generator design corresponds to the configuration intended for operation after thrust modulation is applied, rather than at startup.

As for the "grain wall" boundary, its condition is imposed through a UDF, the operation of which will be described in more detail in the following section.

The summary of the imposed boundary and initial conditions is reported in the Table 4.

Boundary / Region	Condition
Symmetry	Symmetry plane
Pressure outlet	$P_{out} = 1.5 \; MPa$
Wall	Law of the wall (velocity), adiabatic (temperature)
Grain wall	User-Defined-Function
Chamber region (IC)	$P_{CC}=3.0~\mathrm{MPa}$
Outlet region (IC)	$P_{out} = 1.5 \; MPa$

Table 4. Summary of boundary and initial conditions

3.4. The User Defined Function

The UDF controls the " $grain\ wall$ " boundary, depicted in Figure 5. It is written in C, using the framework provided by CONVERGE to enable direct interaction with the solver during the simulation.

The function is executed at each time step. As input, it reads grain-specific data such as the empirical regression coefficients (Equation 20), propellant density, and the associated boundary identifier. It then calculates the area-averaged pressure (at current timestep) at the grain boundary and applies it to determine the grain regression velocity \dot{x}_b using Equation 20. Subsequently, the UDF evaluates the grain mass flow rate \dot{m}_g , displacement Δx_{grain} , and updated remaining mass m_g , as defined in Equations 21, 22, and 23, respectively.

$$\dot{m}_q = \dot{x}_b \cdot A_b \cdot \rho_p \tag{21}$$

$$\Delta x = \dot{x}_b \cdot \Delta t \tag{22}$$

$$m_g = m_g^{t-1} - \dot{m}_g \cdot \Delta t \tag{23}$$

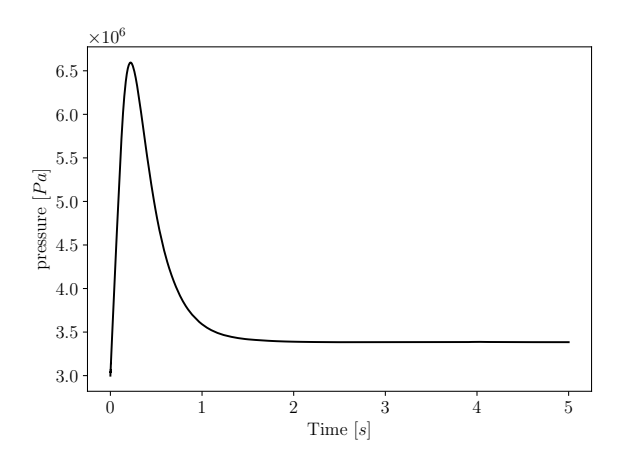
As the grain regresses, the consumed solid propellant injects exhaust gases into the domain. This behavior is modeled within the same UDF, by imposing a per unit volume time species source, Y_{gas} , dependent on the grain velocity \dot{x}_b , as described in Equation 24. The total grain mass flow rate is distributed among boundary-adjacent cells in proportion to their share of the total grain surface area, and converted to a per-volume source term by dividing by the respective cell volume. The temperature of the injected gas is $T_{CC}=2446$ K, as mentioned earlier.

$$Y_{gas} = \frac{\dot{m}_g}{V_{cell}} \cdot \frac{A_{bound}}{A_b} \tag{24}$$

Mesh motion is prescribed by repositioning the grain boundary vertices each time step to their absolute locations based on the total regression distance since ignition, ensuring time-step-independent accuracy and preventing cumulative numerical drift. The grain geometry is defined directly within the UDF, allowing for the flexible implementation of different motion strategies and geometric configurations.

3.5. Simulation Results

Even though the simulation is transient, it exhibits a quasi-steady behavior after the initial startup transient is smoothed out, as shown in Figure 6. This outcome is expected, since the burning cross-section of the grain remains constant over time, leading both the chamber pressure and the regression rate, in Figure 7, to stabilize at steady values. Due to this, the simulation time was limited to the first 5 seconds, until the constant chamber values are reached.



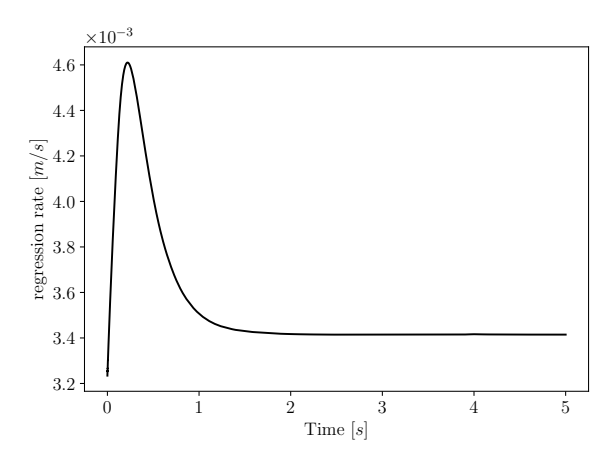
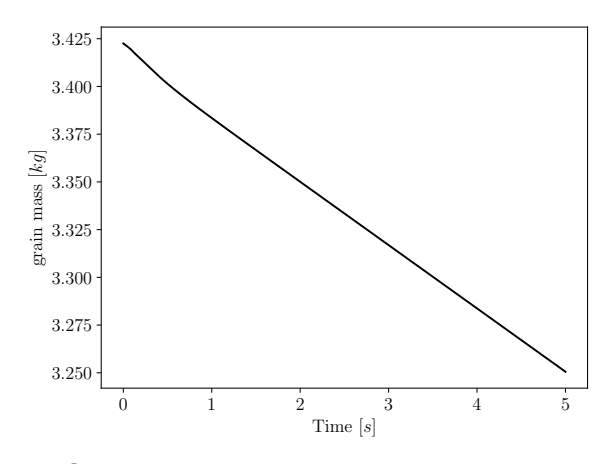


Fig 6. Pressure evolution in the combustion chamber

 $\textbf{Fig 7.} \ \ \text{regression rate trend of the grain surface}$

The chamber pressure for the presented design reached $P_{CC}=33.8$, MPa, with a corresponding regression rate of $\dot{x}_b=3.4$, mm/s. The transient peak observed is not physical and would not be expected under operational conditions; rather, it arises from the chosen initial conditions. The grain mass consumed during this period is shown in Figure 8. Since only a 30° sector was considered, this corresponds to 1/12 of the full grain, giving a total consumed grain mass of $m_{consumed}=2.07$, kg.



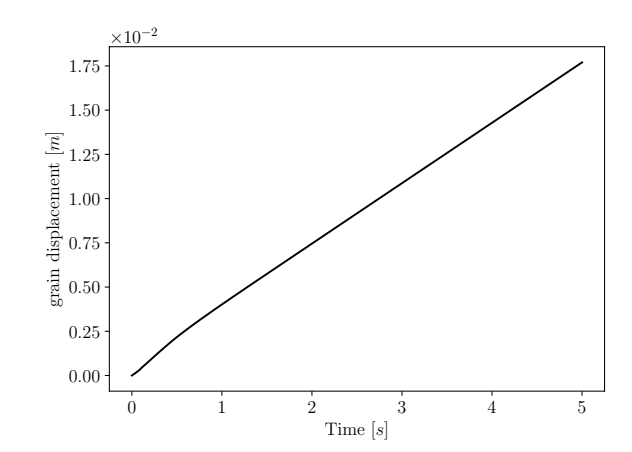


Fig 8. Grain mass consumption, 30° sector

Fig 9. Total axial grain displacement

The grain surface has undergone an axial displacement of $\Delta x = 0.0177$, m, as shown in Figure 9. Owing to the constant burning surface of the grain, both the grain mass and displacement exhibit a linear trend. Even during the short-lived transient peak, the overall behavior remains effectively linear, providing an

accurate representation of the system's behavior.

The amount of grain consumed is shown in Figure 10. The origin of the burning surface was set at z=0, m, which is why the regressed boundary appears in the z<0 region.

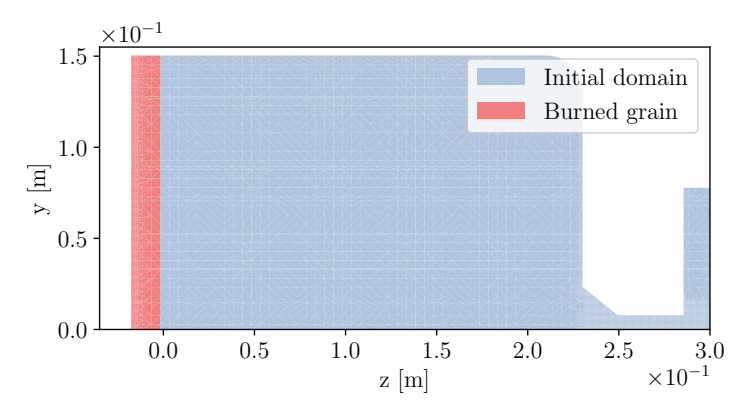


Fig 10. Grain consumed, t = 5s, at 15° slice

The red region, while indicating the total portion of the grain surface that has been consumed, also corresponds to the equivalent number of fluid cells added to the initial domain through the operation of the gas generator, which is confirmed by the overall rising trend of the number of the cells in the chamber region of the domain, shown in Figure 11.

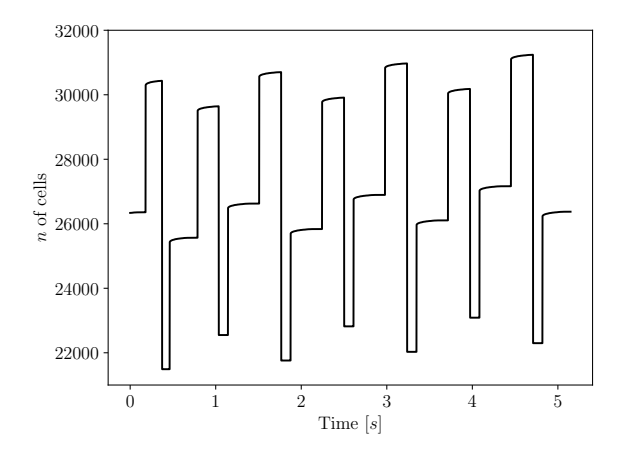


Fig 11. Number of cells in the chamber region

As shown in Figure 12, the chamber successfully pressurizes and enables stable operation of the gas generator. The slice in Figure 13 displays Mach numbers approaching unity along the throat duct, confirming choked flow. The small variations observed arise from viscous and compressibility effects, as well as the influence of downstream expansion, which slightly modifies the near-sonic region upstream. While a finer mesh could provide a more detailed resolution of the throat flow, the primary objective was to capture chamber pressurization via choking. Once choking occurs, the mass flow is dictated by the throat and becomes independent of downstream pressure, ensuring stable chamber conditions despite minor variations within the duct flowfield.

Figure 14 shows the distribution of exhaust gas mass fractions across the computational domain and confirms the correct operation of the UDF, as well as the gas generator, which provides hot, fuel-rich gases for secondary combustion in the ramjet chamber of a supersonic vehicle.

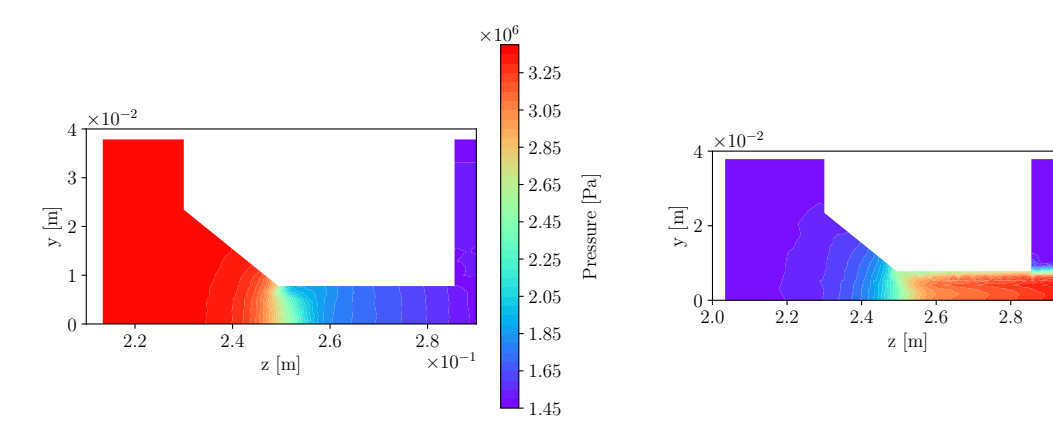


Fig 12. Pressure field in the throat region, t=5s, at 15° slice

Fig 13. Mach number in the throat region, t=5s, at 15° slice

1.12

0.96

0.80

0.64

0.48

0.32

0.16

0.00

3.0

×10

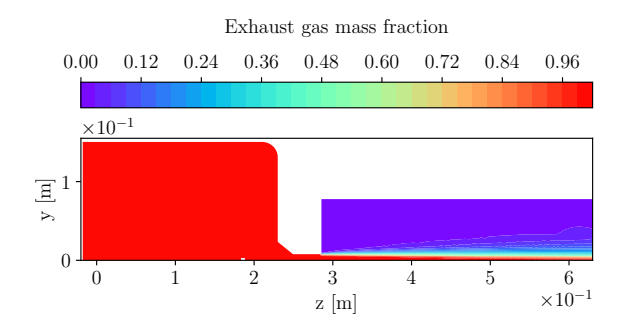


Fig 14. Exhaust gas mass fraction, t=5s, at 15° slice

4. Conclusions

This work presented the modeling and simulation of a solid propellant gas generator for hypersonic airbreathing propulsion. A 0-D lumped parameter model was formulated to describe the transient chamber pressure and grain regression, providing a rapid design and sizing tool. In parallel, a detailed CFD model with a User-Defined Function based on Vieille's law was implemented to capture grain regression and time-dependent geometry evolution. For the selected nozzle throat diameter, the CFD results showed stable pressurization at 33.8 MPa with a regression rate of 3.4 mm/s, linear mass consumption trends, and choked nozzle flow, ensuring steady operation. The exhaust was confirmed to be fuel-rich, meeting the requirements for secondary combustion in a ramjet chamber. Together, the two modeling approaches establish a framework for gas generator design and set the stage for future integration with coupled ramjet simulations and geometry optimization. Future developments will focus on extending the UDF functionalities to enable multi-species injection, allowing the simulation of full secondary combustion. This will support a more complete representation of the ramjet combustion chamber as an integrated system with the gas generator and atmospheric air intake.

References

- [1] Syed Alay Hashim, Srinibas Karmakar, and Arnab Roy. Combustion characteristics of boron-htpb-based solid fuels for hybrid gas generator in ducted rocket applications. Combustion Science and Technology, 191(11):2082–2100, 2019.
- [2] Saugata Mandal, Rakesh Divvela, Syed Alay Hashim, Srinibas Karmakar, and Arnab Roy. Boronladen solid-fueled hybrid gas generator: Its feasibility for potential application in ducted rockets. Combustion Science and Technology, 0(0):1–30, 2025.

- [3] Norman Cohen and Leon Strand. Hybrid propulsion based on fluid-controlled solid gas generators.
- [4] Daniel Komornik and Alon Gany. Investigation of a ducted rocket with a paraffin/oxygen hybrid gas generator. Journal of Propulsion and Power, 35(6):1108–1115, 2019.
- [5] Anil Alan. Pressure control of gas generator in throttleable ducted rockets: A time delay resistant adaptive control approach. Master's thesis, Bilkent University, Ankara, Turkey, June 2017. Available from Bilkent University Institutional Repository.
- [6] Kyung-Hoon Shin, Jongung Won, Hyosung Tak, Sung Choi, Wonbok Lee, and Changjin Lee. A static combustion study on fuel rich propellant for ducted rocket gas generator. 07 2014.
- [7] Hisahiro Nakayama, Yoshiyuki Ikegami, Akihiko Yoshida, Kenji Koori, Kiyoyuki Watanabe, Hidenori Tokunaga, Haruo Shimizu, and Shigeyuki Kanaizumi. Full-Scale Firing Tests of Variable Flow Ducted Rocket Engines Employing Gap Solid Fuel Gas Generator.
- [8] K. J. Richards, P. K. Senecal, and E. Pomraning. CONVERGE 4.1.2. Convergent Science, Madison, WI, 2025. Available at https://convergecfd.com.
- [9] Yogeshkumar Velari, Nikunj Rathi, and P. A. Ramakrishna. Solid fuel-rich propellant development for use in a ramjet to propel an artillery shell. In 8th European Symposium on Aerothermodynamics for Space Vehicles, Lisbon, Portugal, 2021. European Space Agency (ESA).
- [10] Daniil Kalaev, Sasi Kiran Palateerdham, and Antonella Ingenito. Gas generator fuels for solid ramjet: Additive effects and their performance. In 11th European Conference for Aeronautics and Aerospace Sciences (EUCASS), Rome, Italy, 2025. Presented, proceedings not yet published.